

## NUMERICAL TRANSPORT CODES

J.P.H.E.Ongena<sup>1</sup>, I.Voitsekhovitch<sup>2</sup>, M.Evrard<sup>1</sup>, D.McCune<sup>3</sup>

(1) *Laboratorium voor Plasmafysica - Laboratoire de Physique des Plasmas  
Koninklijke Militaire School - Ecole Royale Militaire  
Associatie "EURATOM-Belgische Staat"-Association "EURATOM-Etat Belge"  
B-1000 BRUSSELS (Belgium)  
Partner in the Trilateral Euregio Cluster (TEC)*

(2) *EURATOM/UKAEA Fusion Association, Culham Science Center,  
Culham, OX14 3DB, Abingdon, UK*

(3) *Princeton Plasma Physics Laboratory, Princeton University, P.O.Box 451  
Princeton NJ 08543, USA*

### ABSTRACT

This paper gives a brief introduction on numerical transport codes. The relevant equations that are used in these codes are established, and on the basis of these equations, the necessary calculations needed to resolve them are pointed out. Finally, some examples are given, illustrating their application.

### I. INTRODUCTION

The ultimate aim of plasma fusion research is to reach the conditions for a self-sustained burning plasma. From the Lawson criterion the necessary conditions to reach this objective are well known: we need to confine a plasma for a sufficiently long time at a high temperature and density. However, these plasmas have a natural tendency to reduce temperature and density gradients by particle and heat transport, thus counteracting our efforts to make them hot and dense. Therefore, there is a need for a more detailed understanding of transport processes.

Transport equations describe the temporal and spatial evolution of densities and temperatures, under the influence of external and internal sources and sinks of particles and energy ( $\alpha$ -heating, pellet injection, additional heating, etc...). In applying these equations to the experimental data, by means of so-called transport codes, the transport coefficients corresponding to a given basic set of discharge parameters can be determined in so-called interpretative simulations. The inverse problem can of course also be solved. Given certain theoretical or empirical expressions for the transport coefficients, the behaviour of the plasma densities and temperatures can be predicted in so-called predictive simulations.

In essence, the whole difficulty consists in solving the ion and electron particle and energy balance. However, the solution of these equations requires the knowledge of many additional physical parameters of the discharge. Indeed, some of them are very difficult or impossible to measure, as e.g. neutral density profiles in the discharge, bootstrap currents or charge-exchange losses of the neutral beams, and therefore have to be calculated using adequate physical models. As such, these codes provide, in addition to transport coefficients, quasi automatically a whole series of subsidiary discharge parameters that are derived from the basic input data set and which can then later be compared with the corresponding measured ones.

In this way, transport codes provide a very detailed picture of the discharge, which is at the same time a consistency check of the discharge data and which eventually leads to a better understanding of the transport processes in a plasma.

### II. STRUCTURE OF TRANSPORT CODES.

A description of the transport problem in a general way, i.e. for all different types of devices currently in use to study thermonuclear plasmas, would make this introduction unnecessarily heavy. To get an idea of the complexity of such calculations, it is sufficient to give an outline of the transport problem for one particular device, as the problems encountered are essentially the same for all devices. The description given below will therefore be restricted to tokamak plasmas only.

#### II.A Dimensionality of the problem

Owing to the fact that diffusion and heat transport are much larger along a magnetic surface than perpendicular to it, the problem of plasma transport in magnetically confined plasmas is considerably simplified. This is not surprising, as the charged plasma particles move along the magnetic field lines and thus cover the whole magnetic surface to which they belong. Temperature and density gradients are therefore practically immediately smoothed out along the surface, such that to a good approximation they can be considered as constant on a magnetic surface. In a device with toroidally symmetric magnetic surfaces, such as the tokamak, we therefore can solve all the necessary equations in one poloidal cross-section.

In the case of circular flux surfaces, the problem is obviously one dimensional, with the flux surface radius as independent variable, as all quantities directly related to plasma transport practically only vary perpendicular to the magnetic structure. The poloidal plasma cross section is then divided in a number of  $N$  discrete flux zones and a set of equations is written down for each of these zones.

In the case of a non-circular plasma cross-section, the dimensionality of the transport equations can also be reduced to one. The independent coordinate can now no longer be the flux surface radius, but some other quantity has to be used as an independent coordinate (or in the jargon, flux surface

'label'). In the general case, the 2D MHD equilibrium (Grad-Shafranov) equation:

$$\mathbf{J} \times \mathbf{B} = \text{grad}(P)$$

is solved as a 2D problem, assuming nested flux surfaces and a prescribed boundary or a boundary reconstruction (with magnetic measurements and some diagnostic data from the plasma interior using a code like EFIT[15]) to define the flux surfaces. These are then characterized with a 1D 'label'; in the jargon, these codes are therefore termed 1½ dimensional. Any quantity constant on a magnetic surface can in principle be used as such a 'label'. The different equations are then expressed as a function of this new independent coordinate and averaged over the flux surface zones.

Thus the presence of the magnetic surfaces provides in a general way a 'natural' grid on which the different equations can be solved.

Several transport codes are currently in use, each with a different emphasis on the problems to be solved. TRANSP [1] is a transport code-system and incorporates other packages like NCLASS [2] for the calculation of neoclassical quantities like plasma resistivity, bootstrap current, radial electric fields etc. Another transport code-system is JETTO [3] and this incorporates packages for MHD stability analysis, impurity transport, models to simulate ELMs etc. Other transport codes in use are RITM [4], ONETWO [5] and ASTRA [6] and this list is not exhaustive. The European Task Force 'Integrated Tokamak Modelling' is currently building a new transport code, ETS (European Transport Solver). More information can be found on the website, <http://www.efda-itm.eu/~coelho/efda/EFDA/>. These various codes can be used under rather different environments and platforms, ranging from PCs to clustered networks. The advantage of a cross-laboratory use of transport codes is obvious. It allows standardization in the calculations, leading to an easier exchange in the interpretation of tokamak data analysis. TRANSP and ASTRA are such examples, being routinely used in several labs all over the world. The TRANSP code-system is used for an interpretative analysis of tokamak experiments, i.e. using measured data to deduce transport coefficients. Several codes are used in a predictive mode, e.g. PTRANSF [7], ONETWO, ASTRA in which theoretical and semi-empirical models are used for the transport coefficients, to calculate a set of corresponding plasma profiles for temperature, density, plasma rotation etc. These predictive codes are to be used with care and good knowledge of plasma physics and special attention has to be paid to the algorithms used to ensure sufficient stability.

For the sake of simplicity however, we will restrict ourselves in this introduction to a description of the transport problem in tokamak plasmas with concentric and circular flux surfaces. What follows, is largely based on the transport code TRANSP [1].

## II.B General structure of transport codes

### II.B.1. Electron energy conservation equation

This is the central equation to be solved. If viscosity terms are neglected, this equation may be written as [8]:

$$\frac{3}{2} \frac{\partial}{\partial t} (n_e T_e) + \nabla \cdot \vec{q}_e + \nabla \cdot \left( \frac{5}{2} n_e T_e \vec{v}_e \right) + \vec{v}_i \cdot \nabla (n_i T_i) =$$

$$P_{OH} + P_{add.heat.} - P_{ioniz.} - P_{rad} - Q_{ie}$$

The first term in this equation represents the rate of change of the electron energy, the second term the heat flux losses of the electrons, the third electron convection losses and the fourth represents work done by the plasma particles against the pressure gradient; note that there is discussion about the factor (5/2) in the convection term as it based on the assumption of an ideal gas. However, plasmas are not ideal gases. There is indeed evidence that some cross field transport processes act preferentially on the lower energy, more collisional parts of the thermal ion distribution, with the result that the average convected particle carries a lower amount of energy than would be the case for an ideal gas.

The terms in the right hand side represent the different power gain and loss terms for the electrons:  $P_{OH}$ , given by

$$P_{OH}(r) = \frac{j^2(r)}{\sigma(r)}$$

where  $j(r)$  is the plasma current profile and  $\sigma(r)$  the conductivity, represents the ohmic power;  $P_{add.heat.}$  is the power going to the electrons from any additional heating source (neutral beams, ICRH, ECRH,...).  $P_{ioniz.}$  reflects the power loss by ionisation of a neutral and is equal to (see also Sec II.G) :

$$P_{ioniz.} = n_e n_0 \langle \sigma v \rangle_{ie} W_{ion}$$

where  $n_e$  and  $n_0$  represent the electron density and the neutral atom density in the plasma respectively,  $\langle \sigma v \rangle_{ie}$  the reaction rate is for electron ionisation and  $W_{ion}$  the energy lost by the electron to ionise the neutral atom (13.6eV in the case of hydrogen)

The electron heat flux  $q_e$  is defined as :

$$\vec{q}_e = n_e \chi_e \nabla T_e$$

where

$$n_e \chi_e = \kappa_e$$

is the electron thermal conductivity and  $c_e$  the electron thermal diffusivity.  $q_{ie}$  is the ion-electron equipartition term, given by [9]:

$$q_{ie} = \frac{3 m_e}{m_i} \frac{n_e}{\tau_e} [Z] (T_e - T_i)$$

with

$$[Z] = \frac{1}{n_e} \sum_j \frac{n_j Z_j^2}{A_j}$$

$q_{ie}$  reflects the transfer of power from the electrons to the ions in Coulomb collisions. Finally,  $P_{rad}$  is the power loss of the electrons due to radiation processes.

Thus to solve this equation for the electron heat diffusivity  $\chi_e$  we need at least the following quantities :

- the electron density profile  $n_e(r,t)$
- the electron temperature profile  $T_e(r,t)$
- the ion temperature profile  $T_i(r,t)$
- the profile of the radiated power  $p_{rad}(r,t)$
- the current profile in the plasma,  $j(r,t)$
- the profile of the plasma conductivity  $\sigma(r,t)$
- the radial velocities  $\vec{v}_e$  and  $\vec{v}_i$  of electrons and ions
- the neutral density profile  $n_0(r,t)$
- the power  $p_{add,heat}(r,t)$  from the additional heating going to the electrons

The first five of these quantities can be obtained from different plasma diagnostics:  $n_e(r,t)$  and  $T_e(r,t)$  from the Thomson scattering diagnostic, from interferometric measurements, or electron cyclotron measurements. The ion temperature profile  $T_i(r,t)$  can in principle be obtained from charge-exchange emission spectroscopy, Doppler broadening of impurity lines, or the neutron emission in the case of a Maxwellian plasma. The radiated power  $p_{rad}(r,t)$  is obtained from bolometric measurements. The current profile  $j(r,t)$  can be measured by polarimetric measurements. All the other quantities are not directly available experimentally and have to be calculated. In addition, it is necessary to dispose of an alternative for some of the above-mentioned quantities, for those discharges where some of the data are not very reliable or not available. In what follows we will briefly outline how these calculations can be carried out.

## II.C Magnetics module

The (time varying) current profile in the plasma is obtained by solving the so-called poloidal magnetic field diffusion equation. Upon combining Maxwell's equations (neglecting the terms linked to the displacement current [10])

$$\nabla \times \vec{B} = \mu_0 \vec{J} \quad \text{and} \quad \nabla \times \vec{E} = - \frac{\partial \vec{B}}{\partial t}$$

and substituting :

$$\vec{J} = \sigma(\vec{E} + \vec{v} \times \vec{B})$$

one obtains :

$$- \frac{\partial \vec{B}}{\partial t} = \frac{1}{\mu_0} \nabla \times \left( \frac{1}{\sigma(r,t)} \nabla \times \vec{B} \right) - \nabla \times (\vec{v} \times \vec{B})$$

It can be shown [10] that for the plasmas under consideration, the second term of the left hand side can be neglected. The simplified equation, called the magnetic field diffusion equation due to the close analogy with the heat or density diffusion equation, is then solved with the following boundary conditions (here expressed in cylindrical coordinates):

$$B_p(0) = 0 \quad \text{and} \quad B_p(a) = \frac{\mu_0 I_p}{2\pi a}$$

where  $a$  is the minor radius of the plasma boundary. Note that  $B_p$  is not a flux surface invariant (to convince yourself, think of the case of a divertor plasma, especially when a flux surface approaches a separatrix), and thus in general axisymmetric geometry flux coordinates, the equations are recast in terms of quantities (such as  $\bar{iota} = 1/q$ ) that are flux surface invariants.

The quantity  $\sigma(r,t)$  in this expression is the plasma conductivity. In the simplest approximation, this can be calculated from the input electron temperature and density as follows :

$$\sigma(r,t) = \sigma_{Spitzer} \times C_{NeO}$$

The first factor is the so-called Spitzer conductivity [11,12] the second factor takes into account so-called neoclassical corrections. For the plasmas considered here the Spitzer resistivity  $\eta_{Spitzer}$  resp. Spitzer conductivity  $\sigma_{Spitzer}$  are given by:

$$\eta_{Spitzer} = 2.8 * 10^{-8} T_e^{-1.5} \text{ Ohm-m}$$

$$\sigma_{Spitzer} = (\eta_{Spitzer})^{-1} = 3.6 * 10^7 T_e^{1.5} \text{ Ohm}^{-1} \text{ m}^{-1}$$

with  $T_e$  in keV, and a good approximation to  $C_{NeO}$  is given by [13]:

$$C_{NeO} = \left( 1 - \frac{f_t}{1 + \xi(Z_{eff}) n_{*e}} \right) \left( 1 - \frac{h(Z_{eff}) f_t}{1 + \xi(Z_{eff}) n_{*e}} \right)$$

where  $f_t$  is the trapped particle fraction and  $n_{*e}$  the electron collisionality and  $\xi(Z_{eff})$  and  $h(Z_{eff})$  two polynomial expressions.

The Spitzer or classical conductivity is the conductivity of a cylindrical plasma column. The neoclassical theory, taking into account the toroidal geometry of the plasma, predicts under certain conditions the existence of so-called banana particles, which are trapped in the magnetic field and do not contribute to the plasma current. This effect leads thus to a decrease of the plasma conductivity, which is expressed by the factor  $C_{NeO}$ . This neoclassical correction depends on the collisionality of the electrons,  $n_{*e}$ . In the limit of high collisionality, theory predicts the absence of banana particles and in this case Spitzer conductivity should then apply. Indeed, as  $n_{*e} \rightarrow \infty$ ,  $f_t \rightarrow 0$  and the factor  $C_{NeO}$  tends to 1, but requires the application of numerical codes (e.g. NCLASS) for an accurate evaluation. To test the validity of the Spitzer or neoclassical model for a specific discharge, one can specify whether the neoclassical corrections have to be taken into account or not.

For the calculation of the conductivity, in principle, the profile  $Z_{eff}(r)$ , of the effective ionic charge of the plasma, must be provided. This can be input, but as this is difficult to measure, often an averaged value is computed by iteration, such that the calculated loop voltage (given by the product of the total plasma current with the plasma resistance) is equal to the measured value.

Another important output of this module is the safety factor  $q$ , which is for a cylindrical plasma and large values of

the aspect ratio  $A = R_0/a$ , (with  $a$  the minor and  $R_0$  the major radius of the plasma) given by :

$$q(r) \approx \frac{rB_t^0}{R_0 B_p(r)}$$

where  $B_t^0$  is the value for the toroidal magnetic field on the tokamak axis ( $R=R_0$ ) and  $B_p(r)$  the poloidal magnetic field. For non-circular geometries one uses a more general treatment, by incorporating into the transport code existing, well established stand-alone codes, such as VMEC [14] or EFIT [15]. These can of course also be used for less advanced geometries.

#### II.D Particle balance equation

To obtain a value for the diffusion coefficient and the radial velocities  $\vec{v}_e$  and  $\vec{v}_i$  for electrons and ions, one has to solve the particle conservation equation for the respective particles. This equation is given by

$$\frac{\partial n_\alpha(r,t)}{\partial t} = -\vec{\nabla} \cdot \Gamma_\alpha(r,t) + S_{vol,\alpha}(r,t) + S_{wall,\alpha}(r,t)$$

(with  $\alpha=i,e$  resp. for the ions and the electrons).

$S_{vol,\alpha}(r,t)$  is calculated by modelling possible volume sources (e.g. particle deposition by neutral beams, pellet injection, etc...) and  $S_{wall,\alpha}(r,t)$  by modelling the neutrals originating from the wall. The neutral density profile in the plasma caused by neutral particles released from the wall, is normally calculated by a neutral penetration code. For the latter calculation, we need to specify the energy of the incoming neutrals and their flux or density at the edge and either solve the kinetic equation for neutral distribution function or simulate the neutral behavior using a 3D Monte Carlo procedure.

The particle flux  $\Gamma_\alpha(r)$  in the continuity equation above generally includes the particle diffusion and convection as  $\Gamma_\alpha(r) = -D_\alpha(r) dn_\alpha(r)/dr + n_\alpha(r)v_{r,\alpha}(r)$  with  $D_\alpha(r)$  the diffusion coefficient and  $v_\alpha(r)$  the convective velocity. However, in interpretative simulations where the particle density is measured and the particle sources and sinks are calculated it is not possible to obtain two transport coefficients using only one equation. The simplified approach frequently used in transport analysis of stationary plasmas includes the calculation of the so-called "effective" diffusivity based on the assumption that the convective velocity is zero, i.e.  $\Gamma_\alpha(r) = -D_{\alpha,eff}(r) dn_\alpha(r)/dr$ . Alternatively, the diffusion coefficient and convective velocity can be determined from specifically designed experiments where a very fast variation (or perturbation) of the density is produced on a time scale short enough such that it is safe to assume that  $D_\alpha(r)$  and  $v_\alpha(r)$  remain unchanged. In this way a unique pair of transport coefficients matching the experimentally measured density evolution  $n_\alpha(r,t)$  can be determined. Examples of such experiments include density modulation, single gas puff or NBI blips, laser ablation, etc. This approach has been used to estimate of transport coefficients in trace tritium experiments at JET and will be illustrated in Section III.C.

#### II.E Simulation of additional heating

##### II.E.1 Neutral beam simulation

The most complete description is given by a Monte-Carlo simulation of the neutral beam injection, coupled to a module which solves the Fokker-Planck equation in order to describe the slowing down of the beam particles. Monte-Carlo Fokker-Planck [16] solvers following the actual particle trajectories give a very accurate description but are relatively slow. A considerable faster solution is given by a solver for the bounce averaged Fokker-Planck equation, although it gives a less detailed description of the evolution of the velocity distribution of the injected beam particles and slowing down distribution. Additional outputs of this module are the power deposition profile to ions and electron, the beam shine through power and charge-exchange losses, the fast ion source terms due to ion-ion and ion-electron collisions and charge-exchange with the (slow) plasma background ions, beam driven currents and neutron production rates due to the beam-beam and beam-plasma reactions.

##### II.E.2. Heating with electromagnetic waves: ICRH, ECRH, Lower Hybrid Heating and combined heating scenarios

For each of these heating methods, a separate package has to be developed, which calculates the profile of the power going into the different plasma species. If several heating methods are combined, e.g. ICRH and neutral injection, so-called synergistic effects can play an important role and have to be taken into account.

Several codes are available to calculate the heat deposition of ICRH waves in TRANSP, among them SPRUCE [17] and TORIC [18], where TORIC has become the main workhorse recently. For simplicity of understanding we summarize how SPRUCE was designed and indicate the differences with TORIC. SPRUCE solves a wave equation for  $B_\phi$ , the toroidal component of the magnetic field of the electromagnetic waves, obtained by a reduction of the full set of Maxwell equations by: (i) assuming toroidal symmetry of the problem, which allows to treat each toroidal mode independently and (ii) treating the contributions from the toroidal component of the electric field,  $E_\phi$ , as a small perturbation. (This is true for a pure fast wave but can be wrong when the wave acquires a more electrostatic behaviour as can be the case e.g. when mode conversion occurs). The geometry of the grid used to discretise the equation is completely general and allows for D-shaped and up-down asymmetrical plasma shapes, typical for divertor configurations. The dielectric tensor model currently defined in the code considers bimaxwellian (i.e. non-isotropic) non-relativistic distribution functions for all species, and this to all orders in the Larmor radius expansion. The  $k_\perp^2$  dependency in the dielectric tensor is eliminated by solving the local dispersion relation on each point of the discrete grid, and feeding back the fast wave  $k_\perp^2$  root to each tensor element before using it in the wave equation. This procedure results in unrealistic predictions in the presence of mode conversion, where two roots (or more) are very close to each other. The modes then start to interact by exchanging wave energy. SPRUCE is strictly a single mode or single wave code and its underlying assumptions break down in such a case. To model plasmas where mode conversion occur, from fast wave to ion Bernstein wave or to ion cyclotron wave in the presence of a

poloidal magnetic field from the tokamak (not implemented in SPRUCE), we need to use the code TORIC which is better adapted for those situations.

Once the wave equation is solved, the code determines the power deposition profile, as well as the repartition of the power among the different species. To reduce the CPU time in the calculation, this is done for a single toroidal mode, although the possibility of using a full toroidal spectrum is included in a standalone version of SPRUCE.

Upon termination, SPRUCE or TORIC transfer the wave profiles and power deposition profiles to a Fokker-Planck code for further analysis of the deposited power.

### II.F Ion energy conservation equation

As for the electron conservation equation, we neglect again effects due to viscosity. The ion energy conservation equation can then be written as [8]:

$$\frac{3}{2} \frac{\partial}{\partial t} (n_i T_i) + \nabla \cdot \vec{q}_i + \nabla \cdot \left( \frac{5}{2} n_i T_i \vec{v}_i \right) - \vec{v}_i \cdot \nabla (n_i T_i) = P_{\text{add.heat.}} + P_{\text{neut.}} + Q_{ie} - P_{cx}$$

The different terms in the left-hand side of this equation are analogous to the corresponding ones in the electron energy conservation equation. The same remark applies to the factor 5/2 in front of the third term of the left hand side of the equation;  $p_{cx}$  in the right hand side represents the power loss due to charge exchange of a plasma ion to a neutral and can in a simplified way be written as :

$$p_{cx} = n_i n_0 \langle \sigma v \rangle_{cx} (T_i - T_0)$$

where  $T_0$  is the "neutral temperature" and  $p_{neut.}$  the power gained by ionising a hot neutral. (For more details on  $p_{cx}$  and  $p_{neut.}$  see Sect. II.G)

The ion heat flux  $q_i$  is defined as :

$$\vec{q}_i = n_i \chi_i \nabla T_i$$

where

$$n_i \chi_i = \kappa_i$$

is the ion heat conductivity, and  $c_i$  is the ion heat diffusivity. If the ion temperature profile is known, the profile  $\chi_i(r)$  can be calculated from this equation. In most of the cases the ion temperature is not known at all plasma positions, and a different approach must be followed. One possibility is to input the ion thermal diffusivity (assuming  $\chi_i(r) = a \chi_{i,Neo}(r)$  with  $\chi_{i,Neo}(r)$  a neoclassical expression, or assuming  $\chi_i(r) = a \chi_e(r)$  with  $\chi_e(r)$  the electron diffusivity profile as calculated from the electron energy conservation equation and a multiplier) and calculate the ion temperature profile. The resulting ion temperature profile can then be compared with the values measured at the different plasma positions to check the assumption which was made for  $\chi_i(r)$  or to determine the value of the multiplier  $a$ . In case the neutrons are exclusively due to fusion reactions from the thermal background plasma,

the neutron yield as a function of time could be used in a feedback loop for the ion temperature and a fit can be carried out for the ion temperature profile such as to obtain the number of measured neutrons.

### II.G Modelling of neutral transport

As already indicated in the sections II.B and II.F, the expressions dealing with processes where neutrals are involved, are rather approximate. This section intends to give some more details on how these effects can be modeled in a more realistic way [19]. Processes which cause neutrals to ionize are electron impact ionization, charge-exchange and ion impact ionization. The reaction rate for electron impact ionisation is to a good approximation only dependent on the electron temperature, and the calculation is in principle straightforward. For the other two reactions, there is a conceptual difficulty with the definition of a "neutral temperature", which does not really exist, due to the fact that there are not sufficient collisions between neutrals themselves in order for a Maxwellian distribution to develop. What is usually done in simulations is to subdivide the plasma in a certain number of zones, and assign to the neutrals emerging from charge exchange reactions in each zone an energy equal to 3/2 of the local ion temperature. This approximation is based on the fact that a charge exchange interaction involves in essence only an exchange of electrons, leaving the velocity of the participating particles nearly intact. The emerging neutral has therefore to a good approximation the same velocity as before the reaction, when it was still an ion. The neutral is no longer bound to the magnetic surfaces and its path has then to be followed in a straight line through the plasma until it reionizes again or leaves the plasma.

In presence of neutral beams or pellet injection, an additional source of neutrals is created in the plasma which need to be followed by the code.

The ionisation rates due to charge-exchange and ion impact can then be evaluated as integrals over the neutral energy distribution, weighted by the appropriate rate coefficient, a function of the difference of the energies between the colliding ion and neutral, both of which are known.

In addition the processes of impurity impact ionisation and impurity charge exchange also occur. There are some subtleties here as impurities have more than one charge state. A charge-exchange reaction between a hydrogen neutral and e.g. a  $C^{6+}$  ion, generates a hydrogen ion and a  $C^{5+}$  ion. The result of this reaction is thus two ions, i.e. two particles still bound to the magnetic field lines and this should be taken into account correctly. Such reactions are therefore treated as ionisation reactions in the neutral transport codes.

The work done in ionisation of neutrals is linked to the radiated power loss, as each ionisation reaction is likely to be preceded by decay/excitation reactions, causing radiation to be emitted from the plasma. This effect is most important for partially stripped impurities, as there is more binding energy to work with, one of the reasons why high Z impurities are such a radiation "hazard" for tokamak plasmas. Some specialised codes take these details into account (e.g. MIST [20]), others as TRANSP avoid these details by taking the measured radiated power profiles as an input.

### III. APPLICATIONS AND EXAMPLES OF USE

#### III.A General remarks

Before one is able to reach the final step, where a global consistent picture of the discharge is obtained, a careful preparation of the input data is necessary. A diagnostic could have been out of operation during the experiment, or there could have been some trouble with one or more diagnostics. In the first case we have to look for a replacement of the missing signal in a similar discharge; in the second case one has to find out the cause of the problems, and if possible, correct the measured input data.

A typical transport analysis of a discharge, proceeds therefore in three main stages :

- i. Initial stage : collect as much data of the discharge as possible.
- ii. Preparatory stage : with interpretative analysis, checks are made to ensure the quality of the input data. In case of inconsistencies, a critical check of the data follows.
- iii. Final stage : a full analysis can now be made, i.e. transport coefficients can be calculated, comparisons can be made between the predictions of the code and the actual measurements, etc...

#### III.B Typical outputs and example of analysis.

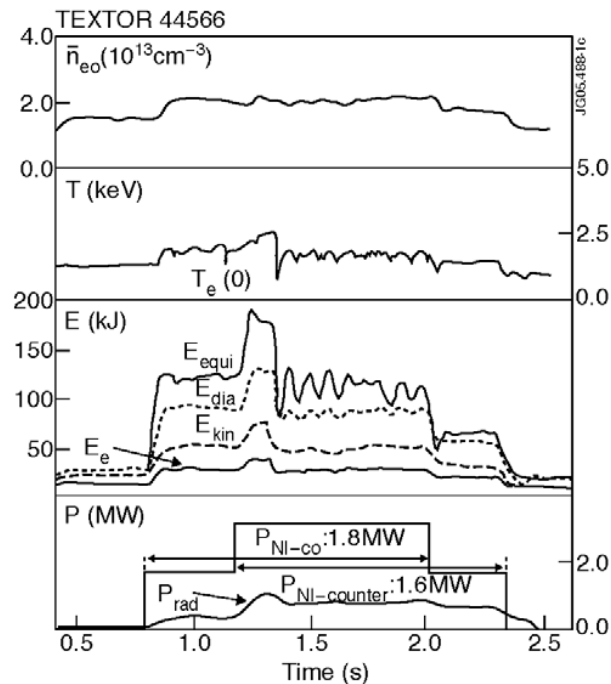


**Figure 1** : Some parameters of TEXTOR discharge 44566. Shown is the time evolution of the central line averaged density, the central electron temperature, different plasma energies, the additional heating power and the power radiated away.

In what follows we show an example of how a transport code can be used to get a better understanding of the physics of a discharge. To this aim we bring in the next section a discussion of part of the output obtained for a discharge heated with CO and counter neutral beam injection (NBI-co, NBI-counter) on the tokamak TEXTOR showing a phase with

improved confinement (I-mode) and L-mode confinement. An overview of the most important discharge parameters is given in Fig. 1 above.

There are three distinct phases in this discharge, a phase with NBI-co injection alone, a phase with combined NBI-co+NBI-counter heating and a phase with only NBI-counter injection. In addition, the combined heating phase showed two different confinement regimes : a short phase, lasting about 150 ms, where an improved confinement was found and a phase of about 650 ms, where L-mode confinement was observed. In what follows, interesting aspects in each of the phases above will be highlighted, in order to get a feeling of what can be learned by the use of transport codes.

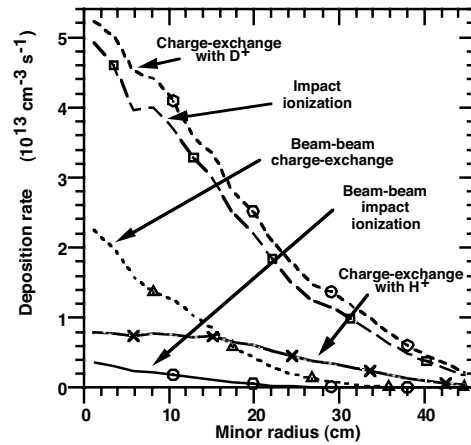


**Figure 2** Deposition rate of beam ions during NBI-CO injection due to: Charge exchange with  $D^+$  background ions (circles, dashed lines); impact ionisation on electrons, ions and impurities and charge exchange with impurities (squares); charge exchange with  $H^+$  background ions (crosses); beam-beam charge exchange (triangles) and beam-beam impact ionisation (circles, full lines).

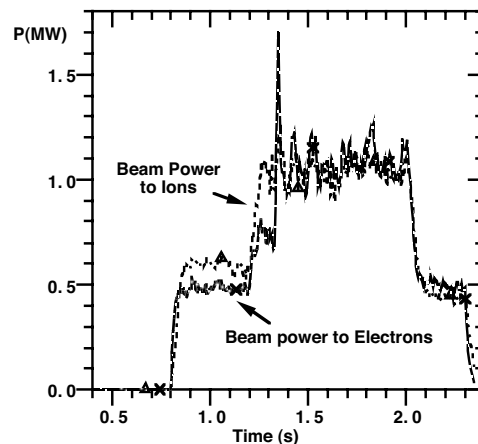


**Figure 3** : Time evolution of the beam power going to ions (triangles) and electrons (crosses).

In Fig. 2, the different contributions to the beam particle deposition are shown during the NBI-co heated phase. Similar figures are obtained during the other phases. The sum of the different terms in this figure is an input to the particle conservation equation for the ions. This figure illustrates the relative importance of the different ionisation reactions to the fast ion formation in the plasma. The beam-beam terms play in this example a minor role.

In Fig. 3, the evolution is shown as a function of time of the beam energy deposition to the ions and the electrons. For the discharge under consideration, we have in the I-mode phase clearly a slightly larger fraction of the beam energy that is going to the ions. The situation changes suddenly at the transition to the L-mode phase, where about equal parts of the beam energy are going to the ions and to the electrons. This is due to the change in the electron temperature of the plasma, which determines the critical energy  $E_c$  ( $E_c \sim T_e$ ). If beam particles are injected with energies above  $E_c$  they will transfer their energy preferentially to the plasma electrons, below this energy they transfer their energy to the ions. As the electron temperature dropped dramatically after the transition, one should then see a larger energy input to the electrons, as is indeed the case. The energy deposition profiles to ions and electrons, inputs to the energy conservation equation are given in Fig. 4.

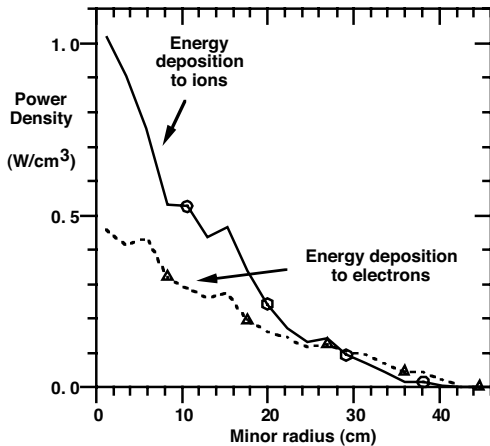


Figure 4: Energy deposition profiles of the neutral beam injection. Shown is the energy deposition profile to the ions (circles) and electrons (triangles).

The presence of fast ionised particles in the plasma is responsible for the presence of large non-inductive, beam-driven currents in the plasma. This is another important output of this package. The evolution of the different plasma currents as a function of time is given in Fig. 5. This illustrative example shows clearly the different effects due to the presence of a beam current in the direction of the plasma current during NBI-co injection, the reduction of the total beam current during combined NBI-co+NBI-counter injection, and a large beam current flowing in the opposite direction of the plasma current during NBI-counter injection.

In addition, the presence of a bootstrap current [21, 22] is predicted. As an illustration, the different current profiles of the plasma during the NBI-co heating phase are given in Fig. 6. The evolution as a function of time of different heating sources of the plasma is given in Fig. 7. We learn from this

figure that only 2.2MW out of 3MW injected beam power is really absorbed by the plasma, the rest is lost by shine-through (fast neutrals which go unionised through the plasma and hit the wall) and by charge-exchange (fast ions which are re-neutralised and leave the plasma as fast neutrals). For an estimate of the confinement time one has to take these effects carefully into account. Note on the same figure the drop in the ohm heating power during the beam heated phase: the high electron temperature (Fig. 1) and the presence of beam driven currents (Fig. 5) during the neutral injection phase lead to a drop in the observed loop voltage.

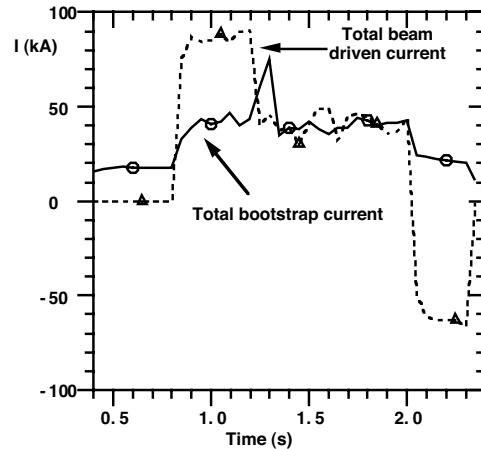


Figure 5: Time evolution of the non-inductive plasma currents: beam-driven current (triangles) and bootstrap current (circles).

The evolution as a function of time of different heating sources of the plasma is given in Fig. 7. We learn from this figure that only 2.2MW out of 3MW injected beam power is really absorbed by the plasma; the rest is lost by shine-through (fast neutrals which go unionised through the plasma and hit the wall) and by charge-exchange (fast ions which are re-neutralised and leave the plasma as fast neutrals). For an estimate of the confinement time one has to take these effects carefully into account.

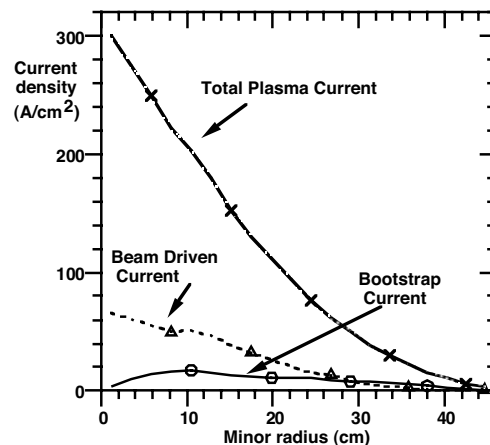


Figure 6 : Radial profile of the total plasma current (crosses), beam driven current (triangles) and bootstrap current (circles) during the-injection phase of the discharge under consideration.

Note on the same figure the drop in the ohm heating power during the beam heated phase: the high electron temperature (Fig. 1) and the presence of beam driven currents (Fig. 5) during the neutral injection phase lead to a drop in the observed loop voltage.

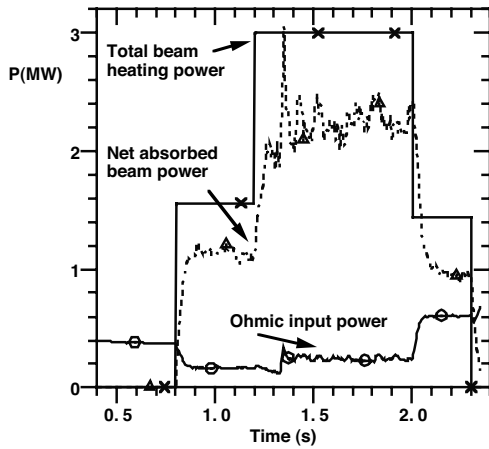


Figure 7 : Time evolution of the different heating powers of the plasma : total injected power (crosses), the net absorbed beam power (triangles) and the ohm input power (circles).

As the total plasma current is feedback controlled to a constant value during the flat top phase of the discharge, a drop in the loop voltage leads thus to a drop in the ohm heating power, being equal to the product of the loop voltage and the total plasma current. These effects have to be taken into account for a realistic estimation of the effective ionic charge from the loop voltage.

The result for the diffusivity values at  $r=0.5a$  (i.e. halfway between the plasma centre and boundary) is shown in Fig.8. The spectacular increase of these values at the transition to the L-mode is clear from this figure.

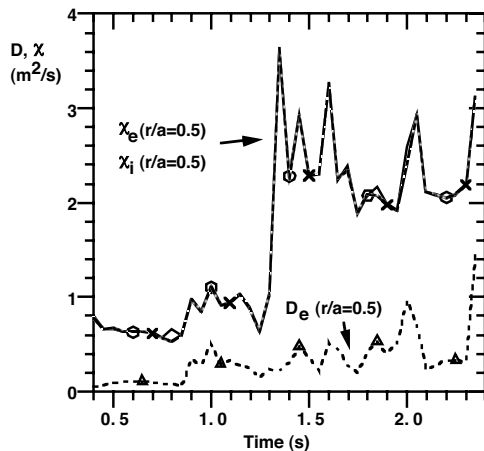


Figure 8 : Time evolution of the central values for the diffusivities of the ions (crosses) and the electrons (circles) and of the diffusion coefficient for the electrons (triangles) at  $r=0.5a$ .

The result of a calculation of the ion temperature assuming  $\chi_i = \chi_e$  during the L-mode phase is given in Fig. 9.

We see very high central temperatures during the improved confinement phase, up to 5 keV, suddenly dropping to about 2.5 keV as soon as the L-mode sets in. A comparison of the electron and ion temperature as a function of time shows that in this discharge the central ion temperature is much higher than the electron temperature: we have to deal with a so called 'hot-ion' mode. The reason for this effect is the central energy deposition of the beam, which is preferentially to the ions in the centre of the discharge, as can be seen in Fig. 4.

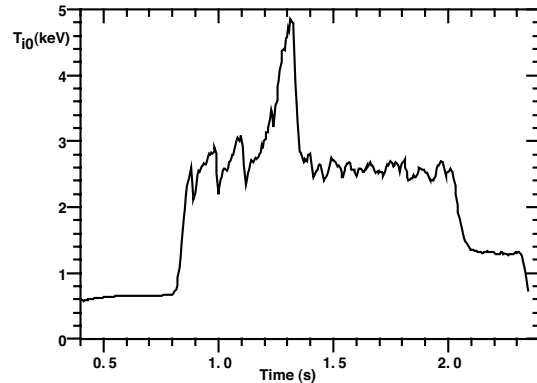


Figure 9 : Time evolution of the calculated central ion temperature, assuming  $\chi_i = \chi_e$

The simulation of the ion temperature profile can be compared with the results of the experiment. This is shown in Fig. 10 for another discharge, similar to the one considered here. The calculations are confirmed by the experimental values at the positions indicated, giving additional confidence in the value of the simulation and in the assumptions made for the ion heat diffusivity.

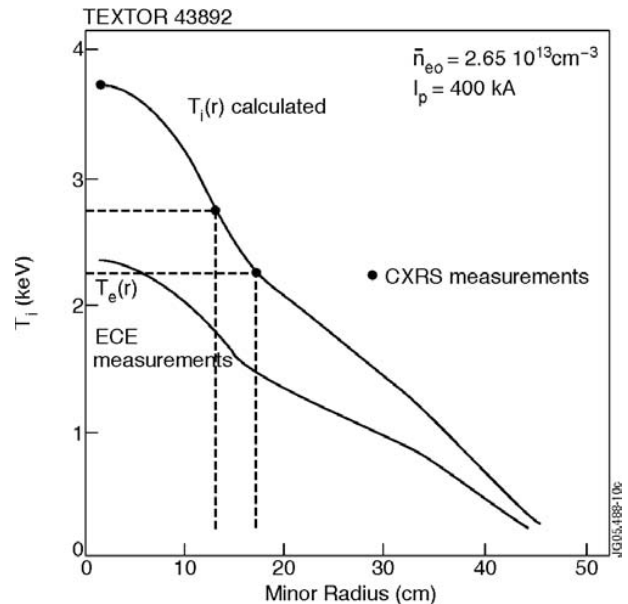
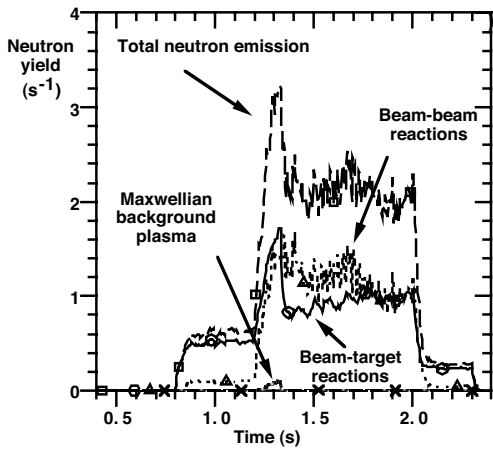


Figure 10 : Comparison of the calculated ion temperature profile with experimental values.



**Figure 11** : Time evolution of the neutron production due to beam-target reactions (circles), beam-beam reactions (triangles) and reactions of the Maxwellian background plasma (crosses). The total neutron production is represented by the dashed line (squares).

The high plasma temperatures in the improved confinement phase of the discharge must have its consequence on the neutron production in the discharge. This is seen in Fig. 11, where the time evolution of the different processes responsible for neutron production is shown. A very high neutron rate is found during the improved confinement phase, suddenly dropping to about half this value during the L-mode phase. We also see that most of the neutrons are due to beam-target reactions, and during the combined NBI-co+NBI-counter phase also for a large fraction to beam-beam reactions, due to the fact that we have then two fast particle streams colliding nearly 'head-on'. The number of neutrons produced by fusion reactions of the Maxwellian plasma ions is negligible in this example. Most often the total predicted neutron rate is compared to a measured value.

And finally different energy confinement times are obtained, as shown in Fig. 12.

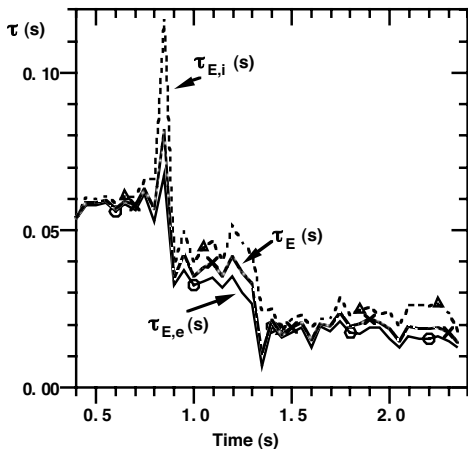


**Figure 12** : Time evolution of different plasma confinement times: the electron energy confinement time (circles), the ion energy confinement time (triangles) and the global energy confinement time of the thermal plasma (crosses).

III.C Trace tritium transport studies at JET

One of the goals of the trace tritium campaign at JET [23] was the estimation of the diffusion coefficient and convective velocity of tritium. For this purpose a very short tritium NBI blip or gas puff from the plasma edge has been applied in deuterium plasmas. As the tritium density is not directly measured, the information about the evolution of the tritium density profile in the plasma has been deduced from the profile of the 14 MeV neutrons produced in the D-T reaction, measured with a neutron camera covering the whole JET cross-section.

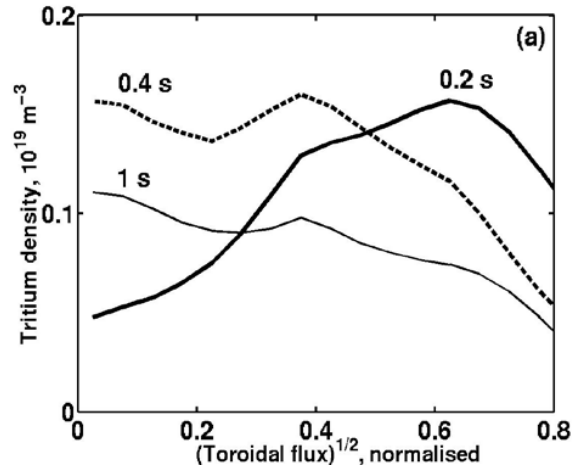
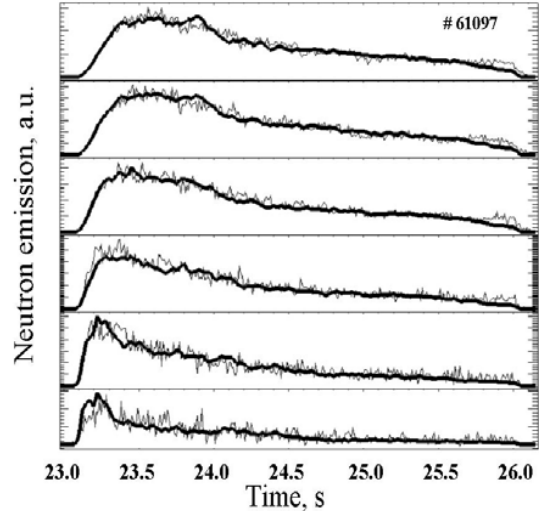


**Figure 13** : JET trace tritium discharge 61097: measured (thin curves) and TRANSP simulation (bold curves) of the neutron emission along the horizontal chords of the neutron camera (top) and tritium density profiles matching the measured neutron emission (bottom). The time after the tritium gas puff for each profile is indicated in the bottom figure [24].

The analysis of these experiments is largely based on transport code simulations. Taking the measured ion temperature and deuterium and impurity density required for the simulations of the neutron emission together with the inferred tritium density, the tritium diffusion coefficient  $D_T(r)$  and convective velocity  $v_T(r)$  have been adjusted in subsequent

simulations with the codes TRANSP and UTC in such a way that the tritium density simulated with these coefficients provides a match of the measured neutron emission along all chords of the neutron camera [24]. A typical result is shown in Fig.13 (top part): agreement between the neutron simulations and measurements and (bottom part): the tritium density profiles at different times after the tritium puff providing this agreement.

#### ACKNOWLEDGMENT

This paper is dedicated to Douglas McCune, a very close friend and colleague from Princeton Plasma Physics Lab. Douglas tragically died in July this year (2011) while participating in a 500 mile bicycle tour "Ride for Runaways", organized as a charity ride for Anchor House, a home for young people in difficulties. Douglas joined this ride for the last 15 years as part of his holidays. Douglas was the genius behind TRANSP and PTRANSF. We will all remember him as a kind and considerate gentleman. He will be very much missed by the worldwide fusion community.

#### FURTHER READING

1. J. BLUM, "Numerical Simulation and Optimal Control in Plasma Physics, with Application to Tokamaks" (Wiley/Gauthier-Villars Series in Modern Applied Mathematics, Chichester) 1989

#### REFERENCES

1. R. J. HAWRYLUK, in *Physics of Plasmas close to Thermonuclear Conditions, Proc. of the Course held in Varenna 1979* (CEC Brussels, 1980), **Vol. 1**, 19-46.
2. W. A. HOULBERG, K. C. SHAIN, S. P. HIRSHMAN, M. C. ZARNSTORFF, *Phys. Plasmas* **4** (1997) 3230
3. G. GENACCHI, A. TARONI. *Report ENEA RT/TIB 1988(5)*, ENEA (1988)
4. M.Z.TOKAR', *Plasma Physics Contr. Fusion* **36**, 1819 (1994).
5. H. E. ST JOHN, T. S. TAYLOR, V. R. LIN-LIU, et al., *Proc. 15th Int. Conf. on Plasma Phys. and Control. Nucl. Fusion Research 1994, Seville Spain*, Vol. 3 (IAEA, Vienna, 1995) p. 603.
6. G. V. PEREVERZEV, P. N. YUSHMANOV, *Report IPP 5/98*, Max-Planck-Institute für Plasmaphysik, 2002
7. R. V. BUDNY, *Nucl. Fusion* **49** 085008 (2009)
8. F. L. HINTON, R. D. HAZELTINE, *Rev. Mod. Physics*, **48**, (2), Part I, 239-308 (1976).
9. S. I. BRAGINSKII, *Reviews of Plasma Physics*, edited by Acad. M.A.Leontovich (Consultants Bureau, New York), **Vol. 1**, 205-311 (1965).
10. J. J. FIELD, in *Plasma Physics and Nuclear Fusion Research*, edited by Richard D. Gill (Academic Press, London) 57-69 (1981).

11. L. SPITZER, Jr. "Physics of fully ionised gases", Second revised edition (Interscience Publishers, New York) 1967.
12. J. WESSON, "Tokamaks", Oxford Science Publications (Clarendon Press, Oxford) 1987
13. S. P. HIRSHMAN, R. J. HAWRYLUK, B. BIRGE, *Nucl. Fusion*, **17**, (3), 611-614 (1977).
14. S. P. HIRSHMAN, D. K. LEE, et al., *Physics of Plasmas*, **1**, (7), 2277-2290 (1994)
15. L. L. LAO, et al., *Nucl. Fusion* **25** 1611 (1985); L. L. LAO, et al., *Nucl. Fusion* **30** 1035 (1990).
16. R.J. GOLDSTON, *J. Comp. Phys.*, **43**, 61-78 (1981).
17. M. P. EVRARD, J. ONGENA, D. VAN EESTER, *Proc. 11th Topical Conference on Radio Frequency Power in Plasmas, Palm Springs 235-238* (1995).
18. M. BRAMBILLA, *Plasma. Phys. Contr. Fusion* **41**, 1 (1999)
19. S. TAMOR, *J. Comput. Phys.*, **40**, 104-119 (1981).
20. R. A. HULSE, *Nucl. Technol. Fusion*, **3**, 259 (1983)
21. R. J. BICKERTON, J.W. CONNOR, J.B. TAYLOR, *Nature Phys. Sci.*, **229**, 110-112 (1971).
22. S. P. HIRSHMAN, *Phys. Fluids*, **21**, (8), 1295-1301 (1978).
23. K.-D. ZASTROW, et al., *Plasma Physics Contr. Fusion* **46** B255 (2004)
24. I. VOITSEKHOVITCH et al, *Phys. Plasmas* **12** 052508 (2005)